Visual Exploration of Complex Functions

Elias Wegert

Abstract The technique of domain coloring allows one to represent complex functions as images on their domain. It endows functions with an individual face and may serve as simple and efficient tool for their visual exploration. The emphasis of this paper is on *phase plots*, a special variant of domain coloring. Though these images utilize only the argument (phase) of a function and neglect its modulus, analytic (and meromorphic) functions are uniquely determined by their phase plot up to a positive constant factor. Following (Wegert in Not AMS 58:78–780, 2011 [49], Wegert in Visual Complex Functions. An Introduction with Phase Portraits, Springer Basel, 2012 [53]), we introduce phase plots and several of their modifications and explain how properties of functions can be reconstructed from these images. After a survey of related results, the main part is devoted to a number of applications which illustrate the usefulness of phase plots in teaching and research.

Keywords Complex functions · Visualization · Special functions · Analytic landscape · Phase plot · Phase portrait · Argument principle · Padé approximation · Riemann zeta function · Gravitational lenses · Filter design

Mathematics Subject Classification (2010). Primary 30-01; Secondary 30A99 · 33-01

1 Introduction

Graphical representations of functions belong to the most useful tools in mathematics and its applications. While graphs of (scalar) real-valued functions can be depicted easily, the situation is quite different for complex functions. Even the graph of a

E. Wegert (✉)
Institute of Applied Mathematics, TU Bergakademie Freiberg,
Akademiestraße 6, 09596 Freiberg, Germany
e-mail: wegert@math.tu-freiberg.de

T. Qian and L.G. Rodino (eds.), *Mathematical Analysis, Probability and Applications – Plenary Lectures*, Springer Proceedings in Mathematics & Statistics 177, DOI 10.1007/978-3-319-41945-9_10

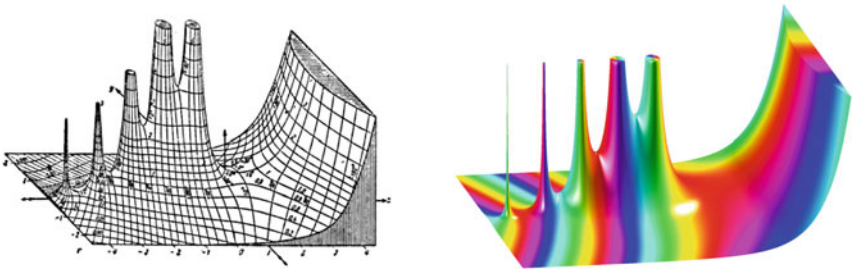

Fig. 1 Analytic landscapes of the Gamma function

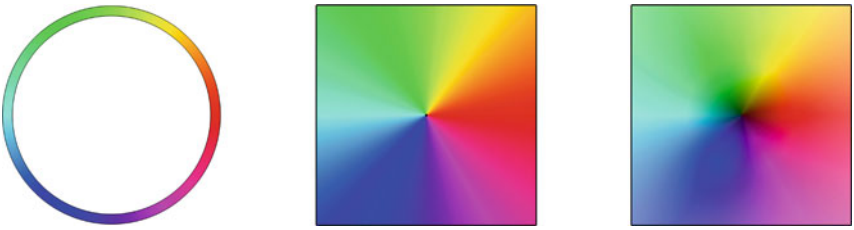

Fig. 2 *Color circle*, coded phase, and domain coloring of $\mathbb{C}$

complex analytic function in one variable is a surface in four dimensional space, and hence not so easily drawn.

The first pictorial representations of complex functions in history are *analytic landscapes*, i.e., graphs of $|f|$; probably introduced by Edmond Maillet [31] in 1903. The analytic landscape of Euler's Gamma function in the famous book [19] by Jahnke and Emde achieved an almost iconic status (see Fig. 1, left). Impressive contemporary pictures of analytic landscapes can be seen on "The Wolfram Special Function Site" [55].

Analytic landscapes involve only the *modulus* $|f|$ of the function f, its *argument* $\arg f$ is lost. In the era of black and white illustrations this shortcoming was often compensated by complementing the analytic landscape with lines of constant argument. Today we can do this much better using *colors*.

Since the ambiguous argument $\arg z$ of a complex number is only determined up to an additive multiple of 2π, we prefer to work with the well-defined *phase* $z/|z|$ of z. Phase lives on the complex unit circle $\mathbb{T}$ and can easily be encoded by *colors* using the standard hsv color wheel (Fig. 2, left). The *colored analytic landscape* is the graph of $|f|$, colored according to the phase of f (Fig. 1, right).

2 Domain Coloring

In practice, it is often difficult to generate analytic landscapes which allow one to read off properties of the function easily and precisely. An alternative approach is not only simpler but even more general: Instead of drawing a graph, one can depict a

function directly on its domain by color coding its values *completely*, as in the image on the right-hand side of Fig. 2.

Such coloring techniques for complex-valued functions have been in use at least since the 1980s (Larry Crone [9], see Hans Lundmark [26]), but they became popular only with Frank Farris' review [10] of Tristan Needham's book "Visual Complex Analysis" and its complement [11]. Farris also coined the name "domain coloring."

2.1 Phase Plots and Their Modifications

In contrast to "standard" domain coloring, which color codes the complete values of f by a *two dimensional* color scheme, *phase plots* display only the phase $\psi(f) := f/|f|$, thus requiring just a *one dimensional* color space with a *circular topology*. To also admit zeros and poles, we extend this definition by $\psi(0) := 0$ and $\psi(\infty) := \infty$, and associate black to 0 and white to ∞, respectively.

At the first glance it seems to be of no advantage to depict the phase of a function instead of its modulus. But indeed there is some subtle asymmetry between these two entities. In fact there are at least three reasons why phase plots outperform analytic landscapes, as can be seen in Fig. 3. First, phase has a small range (the unit circle), while the range of the modulus of an analytic function is usually quite large. As a consequence, the visual resolution is much higher for the phase than for the absolute value.

Second, reconstruction of (missing) information is simpler and more accurate for phase plots, as will be shown in the following section. In particular zeros, poles, and essential singularities can be clearly identified.

Last but not least, the analytic landscape is a three-dimensional object which usually must be projected for visualization, while the phase plot is a flat color image on the domain of the function, which allows one to read off information more precisely.

Since phase occupies only one dimension of the color space (which is usually the three-dimensional RGB space), additional information can be easily incorporated. If, for example, the modulus of f is encoded by a gray scale, we get standard domain

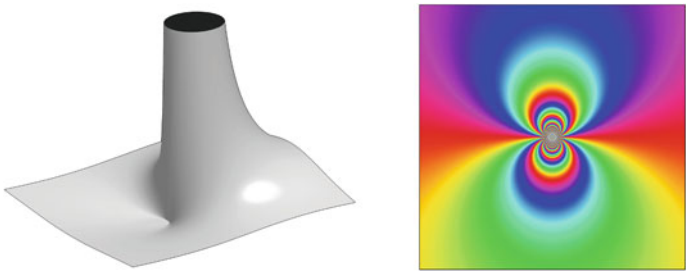

Fig. 3 Analytic landscape versus phase plot of $f(z) = e^{1/z}$

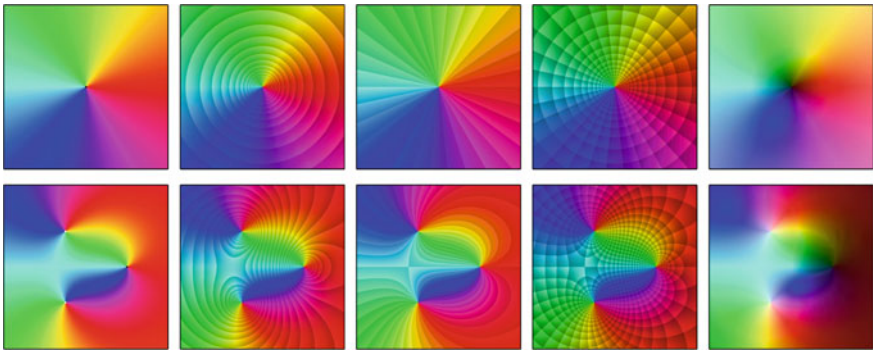

Fig. 4 Color schemes and representations of $f(z) = \dfrac{z-1}{z^2+z+1}$

coloring. Figure 4 illustrates four useful color schemes and the corresponding phase plots of $f(z) = (z-1)/(z^2+z+1)$ in the square $|\mathrm{Re}\, z| < 2$, $|\mathrm{Im}\, z| < 2$. The upper row depicts the color scheme in the w-plane; *pulling back* the colors to the z-plane via the mapping $w = f(z)$ yields the images in the lower row.

The leftmost column corresponds to the pure (plain) phase plot, while the rightmost images show standard domain coloring, respectively. The second column involves a gray component which is a sawtooth function of $\log|f|$, like

$$g = \lceil \log|f| \rceil - \log|f|.$$

Here $x \mapsto \lceil x \rceil$ is the *ceiling function*, which determines the smallest integer not less than x. The jumps in the gray component generate *contour lines* of $|f|$, i.e., lines of constant modulus. In between two such lines darker colors correspond to smaller values of $|f|$. From one line to the next the modulus of f increases *by a constant factor*, which allows one to determine the values much more accurately than from standard domain coloring. Another advantage is that this coloring is insensitive to the range of the function. A similar modification was used in the third column, but here discontinuities of the shading enhance some *isochromatic lines* (sets of constant phase). In the fourth column we have applied both shading schemes simultaneously, which generates a (logarithmically scaled) polar *tiling* of the range plane. The frequencies of the sawtooth functions encoding modulus and phase are chosen such that the tiles are "almost square." Due to the conformality of the mapping, this property is preserved (for almost all tiles) under pull back. This color scheme resembles a *grid mapping*, another common technique for visualizing complex functions. Compared with the standard method of *pushing forward* a mesh from the z-plane to the w-plane, *pulling back* has the advantage that there are no problems with functions of valence greater than one.

It is worth noticing that the shading method works with almost no additional computational costs, is absolutely stable, and does not require sophisticated numerical algorithms for computing contour lines.

2.2 How to Read Phase Plots

Which properties of an analytic function are reflected in its phase plot and how can we extract the information?

First of all it is important to note that *meromorphic* functions are almost uniquely determined by their phase plot: if two such functions (in a connected domain D) have the same phase plot (in an open subset of D), then one is a positive scalar multiple of the other (see [53]).

2.2.1 Zeros, Poles, and Saddle Points

Many features of a complex function can be read off from the local structure of its phase plot: not only zeros and poles of f, but also zeros of f' (saddle points). A simple criterion can be derived from the local normal form $f(z) = a + (z - z_0)^m g(z)$ with $g(z_0) \neq 0$, $a \in \mathbb{C}$ and $m \in \mathbb{Z}$. If z_0 is a zero or a pole of f, we have $a = 0$ (with $m > 0$ or $m < 0$, respectively), otherwise $a \neq 0$ and $m - 1 \geq 0$ is the order of the zero of f'. The following definition is needed in a more precise local classification of phase plots given in [48].

Definition 2.1 A phase plot $P := \psi \circ f$ is said to be (locally) conformally equivalent at a point z_0 to the phase plot $Q = \psi \circ g$ at w_0, if there exists a neighborhood U of z_0, a neighborhood V of w_0, and a bijective conformal mapping φ of U onto V such that $Q\big(\varphi(z)\big) = P(z)$ for all $z \in U \setminus \{z_0\}$.

In this definition, we admit that P and Q are defined only in punctured neighborhoods of z_0 and w_0, respectively.

Theorem 2.2 *Let $f : D \to \widehat{\mathbb{C}}$ be a meromorphic function. Then, for any $z_0 \in D$, the phase plot of f at z_0 is conformally equivalent to the phase plot of the following functions g at 0:*

(i) *If $f(z_0) \in \mathbb{C} \setminus \{0\}$ and $f'(z_0) \neq 0$, then $g(z) = \psi(f(z_0))\, \exp z$.*
(ii) *If $f(z_0) \in \mathbb{C} \setminus \{0\}$ and f' has a zero of order $m \geq 1$ at z_0, then $g(z) = \psi(f(z_0))\, \exp(z^{m+1})$.*
(iii) *If f has a zero of order $m \geq 1$ at z_0, then $g(z) = z^m$.*
(iv) *If f has a pole of order $m \geq 1$ at z_0, then $g(z) = z^{-m}$.*

It follows from (iii) and (iv) that not only the location z_0 but also the multiplicity m of zeros and poles can easily read off from the phase plot of f: in the vicinity of

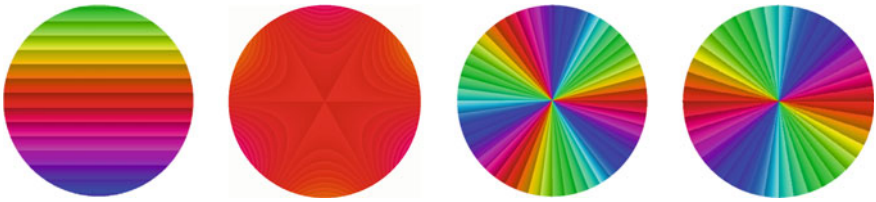

Fig. 5 Local normal forms of (enhanced) phase plots

z_0 it looks like a rotated phase plot of z^m or z^{-m}, respectively. In particular, zeros and poles can be distinguished by the different orientations of colors.

In the second case (ii), the point z_0 is said to be a *saddle* of f of order m. A saddle of order m is the common crossing point of $m+1$ isochromatic lines. In the pure phase plot saddles appear as diffuse spots and it needs some training to detect them. Using a color scheme with enhanced isochromatic lines makes this much easier.

Figure 5 shows the prototypes of (enhanced) phase plots in the four cases with $f(z_0) = 1$, a saddle of order 2 with $f(z_0) = 1$, a zero of order 3, and a pole of order 2, respectively.

2.2.2 Isolated Singularities

It is clear that removable singularities cannot be seen in the phase plot of a function, and we already know how poles look like. So what about essential singularities ? Do they always manifest themselves as in Fig. 3? The answer is basically yes, but the statement of a strict result needs some terminology.

Let $f : D \to \widehat{\mathbb{C}}$ be a nonconstant meromorphic function. For any (color) $c \in \mathbb{T}$, let

$$S(c) := \{z \in D : \psi(f(z)) = c\}$$

be the subset of the domain D where the phase plot of f has color c. After removing from $S(c)$ all points z where $f'(z) = 0$, the remaining set splits into a finite or countable number of connected components. These are smooth curves which we call *isochromatic lines* in the phase plot of f.

Theorem 2.3 *An isolated singularity z_0 of f is an essential singularity if and only if for some (and then for any color) $c \in \mathbb{T}$ any neighborhood of z_0 intersects infinitely many isochromatic lines with color c.*

The result follows from Picard's Great Theorem (see [53]); an elementary proof, based on the Casorati-Weierstrass Theorem, is in [49], Theorem 4.4.6.

We point out that a corresponding result for the lines of constant *argument* does not hold, since the values of $\arg f(z)$ on isochromatic lines with the same color may be different. For example, any continuous branch of $\arg \exp(1/z)$ in $\mathbb{C} \setminus \{0\}$ attains different values on distinct isochromatic lines.

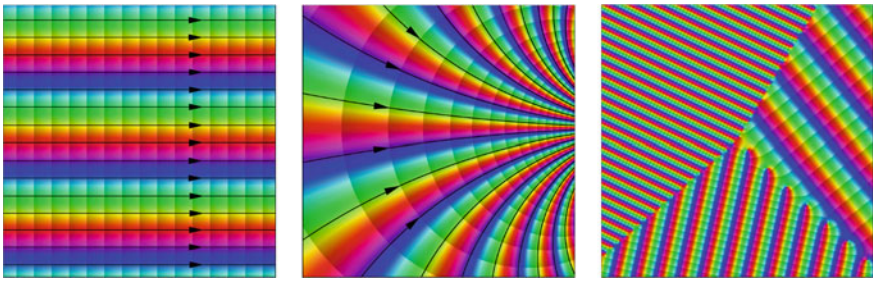

Fig. 6 Phase plots illustrating the growth of functions

2.2.3 Growth

The Cauchy–Riemann equations for (any continuous branch of) the logarithm $\log f = \ln|f| + \mathrm{i}\arg f$ imply that the isochromatic lines are orthogonal to the contour lines $|f| = \text{const}$. Consequently, the isochromatic lines are the lines of steepest ascent/descent of $|f|$. The direction in which $|f|$ increases can easily be determined: for example, when walking on a yellow line in ascending direction, we have red on the right and green to the left.

To go a little beyond this qualitative result, let s denote the unit vector parallel to the gradient of $|f|$ and $n := \mathrm{i}s$. Using the Cauchy–Riemann equations for $\log f$ we get

$$|f'|/|f| = \partial_s \ln|f| = \partial_n \arg f.$$

The left-hand side is the modulus of the logarithmic derivative f'/f; it measures the *growth* of $|f|$ (in the direction of its gradient) relative to the absolute value of f. The right-hand side is the *density of the isochromatic lines*. So, at least in principle, we can read the growth of a function from its (pure) phase plot. In practice it is more convenient to use the enhanced variant with contour lines of $|f|$.

Note that (almost) parallel stripes (with constant density of isochromatic lines) indicate *exponential growth*. The phase plots in Fig. 6 show an exponential function (left), a function growing faster than exponentially from left to right (middle), and the sum of three exponential functions e^{az} with different complex values of a. Knowing the size of the depicted domain, an experienced observer can read off the three values of a.

2.2.4 Periodic Functions

Clearly, the phase of a (doubly) periodic function is (doubly) periodic, but what about the converse? If, for example, a phase plot is doubly periodic, can we then be sure that it represents an elliptic function?

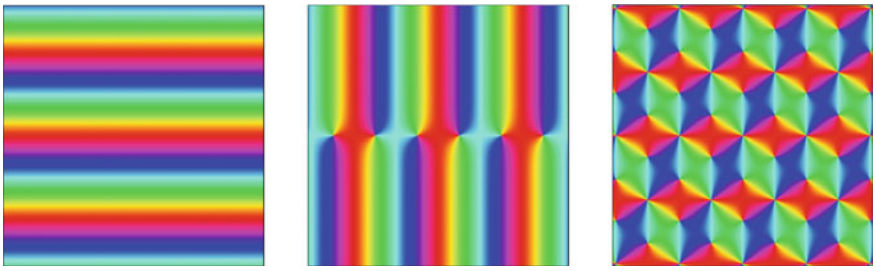

Fig. 7 Three prototypes of periodic phase plots

Though there are only *two* classes (simply and doubly periodic) of nonconstant periodic meromorphic functions on $\mathbb{C}$, we can observe *three* different types of periodic phase plots as shown in Fig. 7 (from left to right: an exponential function, the cosine function and a Weierstrass $\wp$-function).

Motivated by these pictures we say that a (nonconstant) phase plot P is

(i) *striped* if there exists $p_0 \neq 0$ such that for all $p = \alpha p_0$ with $\alpha \in \mathbb{R}$

$$P(z + p) = P(z) \text{ for all } z, \tag{2.1}$$

(ii) *simply periodic* if there exists $p_0 \neq 0$ such that (2.1) holds if and only if $p = k\, p_0$ for all $k \in \mathbb{Z}$,

(iii) *doubly periodic* if there exist $p_1, p_2 \neq 0$ with $p_1/p_2 \notin \mathbb{R}$ such that (2.1) holds if and only if $p = k_1 p_1 + k_2 p_2$ for all $k_1, k_2 \in \mathbb{Z}$.

While it is easy to characterize striped and simply periodic phase plots, the doubly periodic case is more subtle. In the following theorem σ denotes the Weierstrass Sigma function:

$$\sigma(z) := z \prod_{\lambda \in \Lambda \setminus \{0\}} \exp\left(\frac{z}{\lambda} + \frac{z^2}{2\lambda^2}\right)\left(1 - \frac{z}{\lambda}\right),$$

where $\Lambda := p_1\mathbb{Z} + p_2\mathbb{Z}$ is the grid generated by the primitive periods p_1 and p_2. We further define u_1, u_2 and q_1, q_2 by

$$u_j := \sum_{\lambda \in \Lambda \setminus \{0, p_j\}} \frac{1}{\lambda(\lambda - p_j)^2}, \qquad q_j := p_j^2 u_j - 3/p_j. \tag{2.2}$$

Theorem 2.4 *The phase plot of a nonconstant meromorphic function f on $\mathbb{C}$ is*

(i) striped *if and only if there exist $a, b \in \mathbb{C}$ with $a \neq 0$ such that*

$$f(z) = \mathrm{e}^{az+b},$$

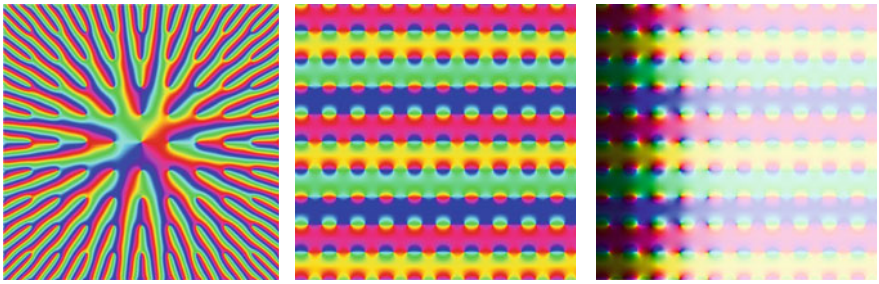

Fig. 8 A Weierstrass Sigma function σ and $\sigma(z)/\sigma(z-b)$

(ii) simply periodic *with primitive period p if and only if there exist a simply periodic function $g : \mathbb{C} \to \mathbb{C}$ with period p and a real number a such that*

$$f(z) = \mathrm{e}^{az/p}\, g(z),$$

(iii) doubly periodic *with primitive periods p_1 and p_2 ($p_1/p_2 \notin \mathbb{R}$) if and only if f can be represented as*

$$f(z) = \mathrm{e}^{az}\, g(z) \frac{\sigma(z)}{\sigma(z-b)},$$

where g is elliptic with periods p_1 and p_2, and $a, b \in \mathbb{C}$ satisfy

$$\mathrm{Im}\,(ap_j) \equiv \mathrm{Im}\,(bq_j) \pmod{2\pi}, \qquad j = 1, 2,$$

with q_j defined in (2.2).

For a proof of (i) and (ii) see [53], assertion (iii) is due to Marius Stefan [40].

Figure 8 shows a Weierstrass Sigma function and a quotient $\sigma(z)/\sigma(z-b)$ which has a doubly periodic phase plot (middle), but is not an elliptic function (right).

3 Phase Diagrams

The phase plot of a function contains information which is nonlocal. As an example, we consider the *argument principle*: Let $f : D \to \widehat{\mathbb{C}}$ be meromorphic in the domain D and assume that D contains the closure of the interior of a (positively oriented) Jordan curve J. If f has neither zeros nor poles on J, then the winding number $\mathrm{wind}_J P_f$ (about the origin) of the phase $P_f := \psi \circ f$ along J is the difference of the number $n(f, J)$ of zeros and the number $p(f, J)$ of poles of f inside J (counted according to their multiplicity),

$$n(f, J) - p(f, J) = \mathrm{wind}_J P_f.$$

This number can easily be read off from the phase plot of f, and we call it the *chromatic winding number* of f along J. In the image on the left-hand side of Fig. 9 we have $\mathrm{wind}_J P_f = 4$. The phase plot in the middle reveals that the interior of J indeed contains four zeros (one is double) and no poles of f.

But this is not yet the end of the story, one can discover even more. In the next section we follow [48].

3.1 The Phase Flow

The isochromatic lines in the phase plot of f are the flow lines of the vector field

$$V_f : D \to \mathbb{C},\ z \mapsto -\frac{f(z)\,\overline{f'(z)}}{|f(z)|^2 + |f'(z)|^2}$$

(see Fig. 9, middle and right). With an appropriate definition at zeros and poles of f the vector field V_f is smooth and vanishes exactly at the zeros and poles of f and f', which we call *singular points* of V_f.

The flow generated by the vector field V_f is said to be the *phase flow* of f. Endowing the phase plot with the orbits of this flow yields the *phase diagram* of f. Using standard techniques from the theory of dynamical systems, one can characterize the *orbits* of V_f and describe the *basins of attraction* of zeros (for details see [48]).

3.2 The Extended Argument Principle

If J is a Jordan curve in D which does not contain singular points of V_f, the *directional winding number* $\mathrm{wind}_J V_f$ of f along J is the winding number (about the origin) of V_f along J. In the rightmost image of Fig. 9 we have

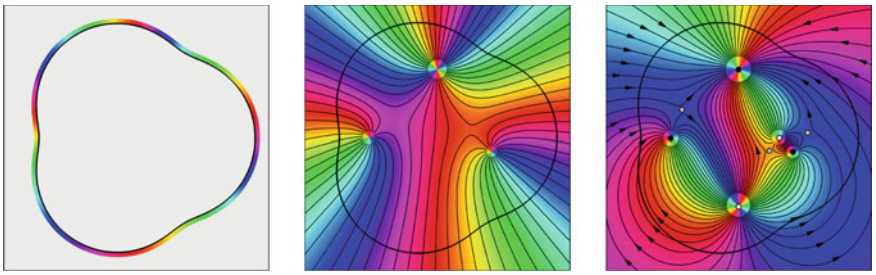

Fig. 9 Argument principle, phase flow and winding numbers

$$\mathrm{wind}_J P_f = 1, \qquad \mathrm{wind}_J V_f = 2.$$

Analyzing the phase diagram using index theory reveals a relation between the two winding numbers of f along J and the numbers $n(f', J)$ and $p(f', J)$ of zeros and poles of f' inside J, respectively.

Theorem 3.1 ([48]) *Let f be meromorphic in D and assume that the positively oriented Jordan curve J and its interior are contained in D. If neither f nor f' have zeros or poles on J, then*

$$n(f', J) - p(f', J) = \mathrm{wind}_J P_f - \mathrm{wind}_J V_f$$

Note that (at least in principle, but not always in practice) both winding numbers can be read off from the phase plot of f in an arbitrarily small neighborhood of J.

If f is holomorphic, the argument principle and Theorem 3.1 allow one to determine the number of zeros of f and f' inside J from the phase plot of f near J. In Fig. 9 (left) we have $\mathrm{wind}_J P_f = 4$ and $\mathrm{wind}_J V_f = 1$, so that $n(f, J) = 4$ and $n(f', J) = 3$.

An important special case pertains to the situation when f is holomorphic and the isochromatic lines of f are nowhere tangent to J. Since the latter implies $\mathrm{wind}_J V_f = 1$, Theorem 3.1 tells us that then $n(f', J) = n(f, J) - 1$. This yields a short proof of Walsh's theorem on the location of critical points of Blaschke products [46–48].

4 Applications

In this section we discuss applications of phase plots which we believe to be useful—though in some examples the mathematical background is rather trivial.

4.1 Software Implementation

When one needs to compute special functions numerically, it is tempting to download code which is freely available on the internet. In many cases this may be an easy and efficient way to solve the problem, but one should be aware that there is no guarantee that software does what it claims to do.

An example is shown in Fig. 10. The image on the left is a phase plot of the complex Gamma function, computed with a certified Matlab routine. The picture in the middle displays the phase plot of a want-to-be Gamma function in the same domain, computed with code from a dubious source. Though the overall impression is almost the same, a closer look reveals that something must be wrong on the negative real axis near the left boundary of the domain. Zooming in a little closer, we discover a beautiful bug sitting at the end of an artificial branch cut.

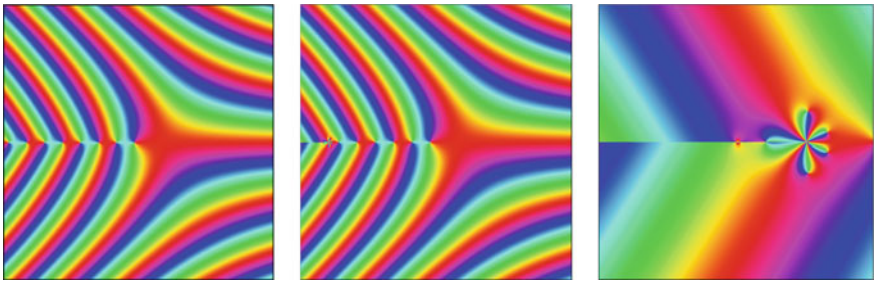

Fig. 10 A bug in software for evaluating the Gamma function

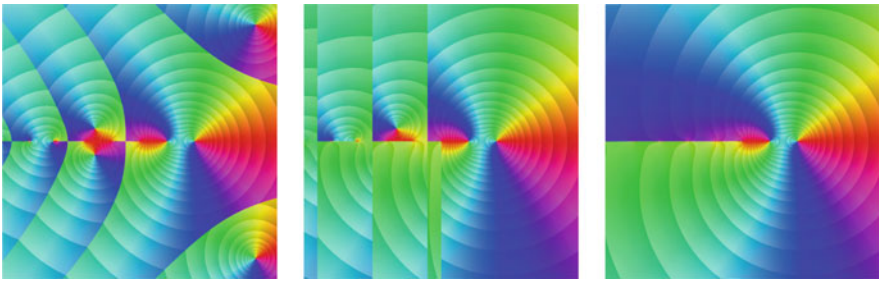

Fig. 11 Implementations of the logarithmic Gamma Function

Since this is not the only incident which can be reported, one should be very careful when using software without knowing what it really computes. Though looking at phase plots can by no means ensure correctness of computations, it may help to discover some inconsistencies quite easily.

4.2 Multivalued Functions

Computations involving multivalued functions, like complex nth roots or the complex logarithm, are often challenging because usually only their main branch is implemented in standard software. In particular, composing such functions without taking care for choosing the appropriate branches may lead to fallacious results.

Let us consider the logarithmic Gamma function `GammaLog`(z) as an example. The three images of Fig. 11 show $\log\Gamma(z)$ (left), another implementation from the web which claims to be `GammaLog`(z) (middle), and a version having a branch cut along the negative real line (which is the standard definition). After some training, phase plots make it quite easy to understand the structure of spurious branch cuts, but removing them can be very tedious.

4.3 Riemann Surfaces

Phase plots may serve as convenient tool for constructing Riemann surfaces. We demonstrate this for the Riemann surface of the inverse of the sine function $f(z) = \sin z$. Basically this procedure involves three steps:
Step 1. Look at the phase plot of f in the z-plane and determine the basins of attraction of the zeros (first row of Fig. 12). In the case at hand the basins are vertical stripes $k\pi < \operatorname{Re} z < (k+1)\pi$, $k \in \mathbb{Z}$. Every such basin is mapped onto a copy of the complex w-plane, slit along the rays $[-\infty, -1]$ and $[1, +\infty]$ (second row).
Step 2. Change the coloring of the z-plane to the standard color scheme (phase plot of the identity, see first row of Fig. 13).
Step 3. Push the colors forward from the fundamental domains to the w-plane by $w = f(z)$. This generates phase plots of f^{-1} on the different sheets of its Riemann surface (second row of Fig. 13).

Gluing the rims of branch cuts according to their neighboring relations (which usually, but not always, can be seen from the phase plots), yields the Riemann surface on which the phase plot of g can be displayed (see Fig. 14).

Thomas Banchoff [5] and Michael Trott [43, 44] described techniques for visualizing complex functions on domain-colored Riemann surfaces. This topic was studied in more detail by Konrad Poehlke and Konstantin Polthier [33]. In two subsequent papers [34] and [32] (with M. Niesen) they propose algorithms for the automatic construction of Riemann surfaces with prescribed branch points and branch indices.

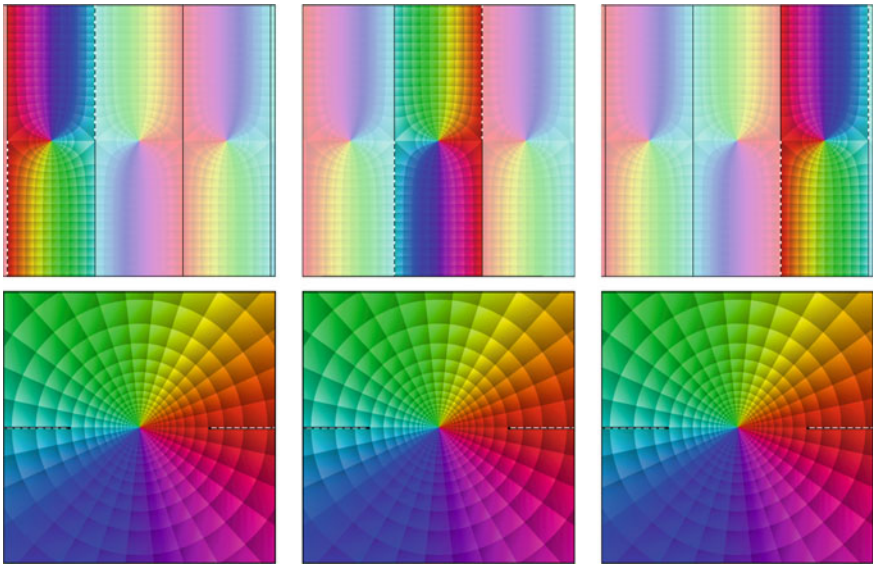

Fig. 12 The sine function mapping strips to $\mathbb{C}$

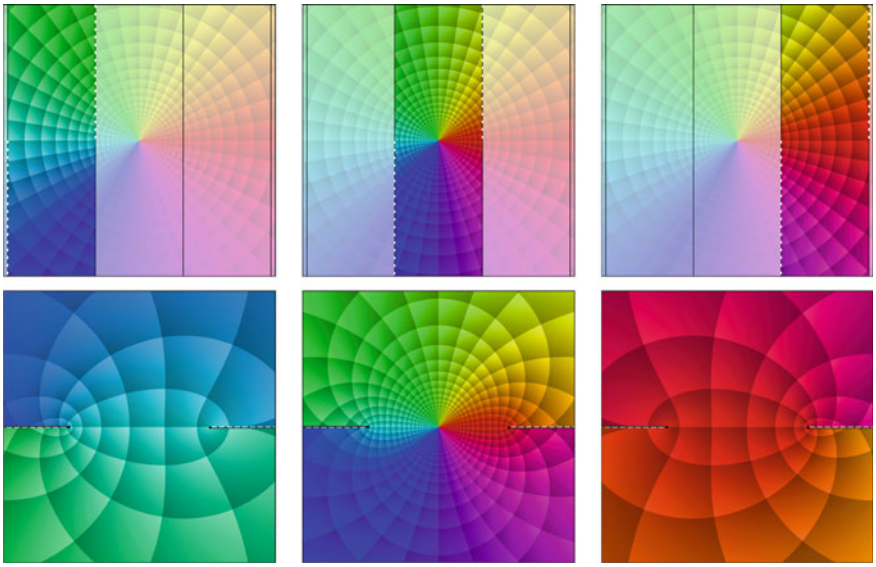

Fig. 13 Three branches of the inverse sine function

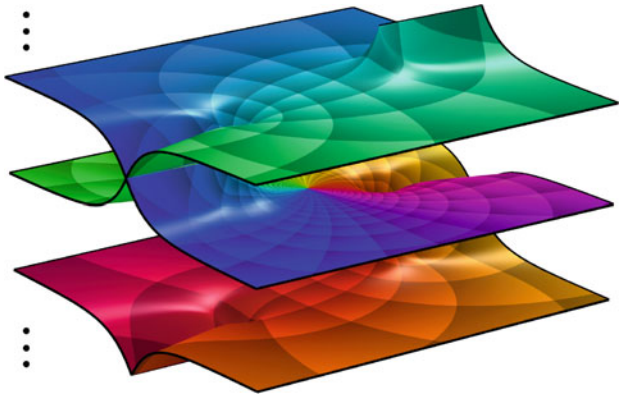

Fig. 14 The inverse sine function on its Riemann surface

The image on the left of Fig. 15 (reproduced from [32] with permission) shows such a surface composed of five sheets.

Another (more specialized) approach to automated computation of Riemann surfaces of algebraic curves is described in Stefan Kranich's PhD thesis [24]. The image on the right of Fig. 15 is the Riemann surface of the folium of Descartes, defined implicitly by the equation $z^3 + w^3 - 3zw = 0$ (reprinted in scaled form with permission).

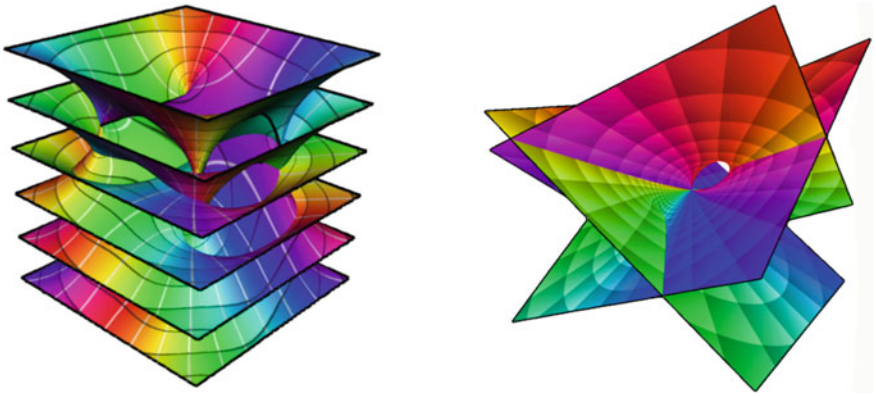

Fig. 15 Automatically generated Riemann surfaces

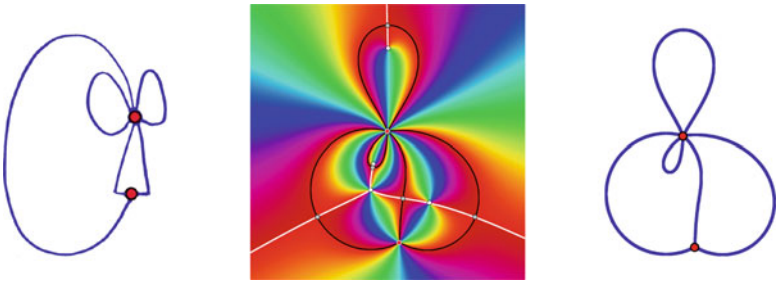

Fig. 16 Canonical embedding of planar graphs via Belyi functions

A general point-based algorithm for rendering implicit surfaces in $\mathbb{R}^4$ using interval arithmetic for topological robustness and (phase) coloring as substitute for the fourth dimension is described by Bordignon et al. [7].

4.4 Belyi Functions

A planar graph can be embedded in the (complex) plane in many different ways. Given one such embedding (like the one on the left-hand side of Fig. 16), one may ask whether it can be continuously deformed into a "canonical shape" without changing the vertex–edge relation and with no crossings throughout this whole process. Surprisingly, such a representation exists (depicted on the right of Fig. 16). A theorem due to Gennadii Belyi [6] tells us that every planar graph G can be represented by a rational function R (in the special class of so-called Belyi functions) with the following properties: The zeroes of R are exactly the vertices of G (red points) and the edges of G (black lines) are the preimages of the interval $[0, 1]$ under R. In every

face of G there is exactly one pole of R (white points) and the preimages of $[1, +\infty]$ (white lines) connect the poles to one point (gray) on each of the edges bounding the face containing that pole. (The area outside the graph is considered to be a face with its pole at infinity.) Moreover, all edges run into a vertex with equal angles between neighboring edges and the (white) lines originating at the poles intersect the edges perpendicularly. Last but not least, every face is the basin of attraction (see Sect. 3 and [48]) of the associated pole (with respect to the reverse phase flow).

The actual computation of the Belyi function associated with a given graph is a challenging problem. Donald Marshall developed an approach via conformal welding [27, 28] and implemented it using his software ZIPPER [29, 30]. I am grateful to him for providing the coefficients of the Belyi function shown in Fig. 16.

4.5 *Filters and Controllers*

In signal and control theory (linear, causal, time invariant, and stable) systems are described by transfer functions, which are analytic in the right half plane. In practice, most transfer functions are rational functions with poles in the left half plane. In the frequency domain the system acts on an input as multiplication operator with its transfer function T. In particular, the frequency response $T(\mathrm{i}\omega)$ tells one what the system does with harmonic input signals $\mathrm{e}^{\mathrm{i}\omega t}$: The values $|T(\mathrm{i}\omega)|$ and $\arg T(\mathrm{i}\omega)$ are the *gain* and the *phase shift* induced by the system operating at frequency ω.

The phase plot on the left of Fig. 17 is the transfer function of a Butterworth filter—a low pass filter, which damps high frequency signals. This can be seen from its frequency response on the imaginary axis: the white segment is the passband where $|T(\mathrm{i}\omega)| \approx 1$, in the stopband (black) $|T(\mathrm{i}\omega)|$ decays for increasing values of ω. Using the contour lines and the phase coloring one can read off the frequency response directly from the phase plot of T and, for instance, construct Bode and Nyquist plots.

Santiago Garrido and Luis Moreno [15] developed more elaborate techniques involving phase plots for designing controllers. The two images in the middle and

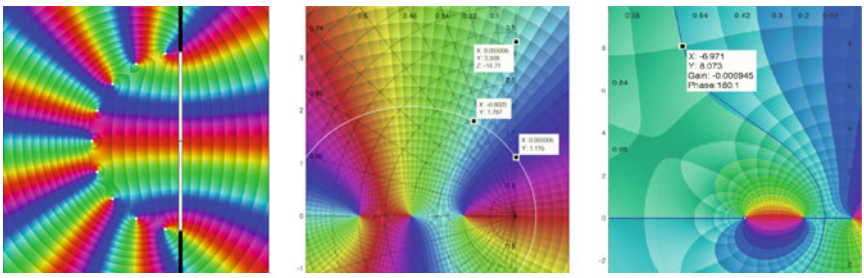

Fig. 17 Design of filters and controllers

on the right of Fig. 17 show some screenshots from their software (I am grateful to the authors for providing these images).

4.6 Numerical Algorithms

In recent years, domain coloring techniques have proven useful tools in analyzing numerical algorithms. Compared with numerical values, like the norm of the error (function) of an approximate solution, images deliver much more structural information. This may, for instance, improve the understanding of the method's global behavior. A further advantage of phase plots is the high sensitivity of the phase $\psi(z)$ for small values of z, which lets them act as a looking glass focused at the origin.

4.6.1 Iterative Methods

Numerical methods often use iterative procedures to find successively better approximations to solutions of a problem. There are many options to display relevant information about the global behavior of these methods. In order to demonstrate how coloring techniques can be used in this context, we consider zero finding for a complex function f (for a more detailed exposition see Varona [45]).

Most iterative methods start with an initial value z_0 and calculate $z_1, z_2, \ldots$ recursively by

$$z_{k+1} = z_k - \lambda_k \, f(z_k), \tag{4.1}$$

where λ_k is a parameter which may be constant (Whittaker's method) or depending on z_k. For $\lambda_k := 1/f'(z_k)$ we get the popular Newton method which converges (locally) quadratically. A skillful choice of λ_k leads to an accelerated convergence of the approximating sequence. For example, the "double convex acceleration of Whittaker's method" (DCAW method) uses the iteration formula (see [18, 45])

$$z_{k+1} = z_k - \frac{f(z_k)}{2\,f'(z_k)} \left[1 - g(z_k) + \frac{1 + g(z_k)}{1 - g(z_k)\big(1 - g(z_k)\big)} \right],$$

where $g(z) = f(z)\,f''(z)/\big(2f'(z)^2\big)$. This method has convergence order 3.

Figure 18 displays the results of some experiments for solving $f(z) := z^5 - 1 = 0$ by the recursion (4.1). We see the fourth iterate z_4 (upper row) and the residue $f(z_4)$ (lower row) as functions of the initial point z_0 for different methods, namely (from left to right) Whittaker's method with $\lambda = 0.15$, Newton's method, an accelerated Whittaker method (see [45]), and the DCAW method.

The pictures in the upper row are plain phase plots, showing the emanating basins of attraction of the zeros; the five dominating colors correspond to the phase of these zeros. In the lower row we used domain coloring, encoding the modulus by a gray

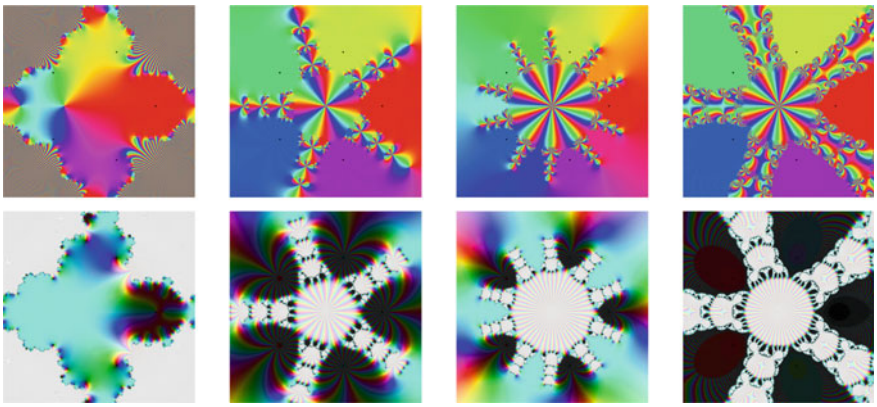

Fig. 18 Iterates and residues for several zero-finding methods

scale, to get a better feeling for the magnitude of the residue. In the (almost) black regions the absolute value of $f(z_4)$ is in the range of 10^{-15}, in the bright domains the iterates converge to the point at infinity.

4.6.2 Numerical Differentiation

As another simple example, we consider approximations of the first derivative of a function f by the difference quotients

$$f_1(z) := \frac{f(z+h)-f(z)}{h}, \qquad f_2(z) := \frac{f(z+h)-f(z-h)}{2h},$$
$$f_3(z) := \frac{f(z+\mathrm{i}h)-f(z-\mathrm{i}h)}{2\mathrm{i}h}, \qquad f_4(z) := \frac{f_2(z)+f_3(z)}{2}.$$

Figure 19 shows phase plots of the error functions $f' - f_k$ $(k = 1, 2, 3, 4)$ for $f(z) = 1/z$ with $h = 10^{-3}$ (first row) and $h = 10^{-5}$ (second row). What do we see here?

The difference quotients f_k approximate f' with order h^n, where $n = 1, 2, 2, 4$ for $k = 1, 2, 3, 4$, respectively. A straightforward computation using Taylor series then shows that the error function satisfies

$$e_k(z) := f_k(z) - f'(z) = c_k\, h^n\, f^{(n+1)}(z) + O(h^{n+1})$$

so that we basically should see a phase plot of $c_k\, f^{(n+1)}(z) = c_k(-z)^{-n-2}$. This is indeed the case in the first three pictures for $h = 10^{-3}$. For f_4 the error is already so small, that rounding effects (cancelation of digits) manifest themselves near the boundary. For $h = 10^{-5}$, similar effects can also be observed for e_2 and e_3, while in the fourth picture the error function e_4 is completely dominated by noise (for a

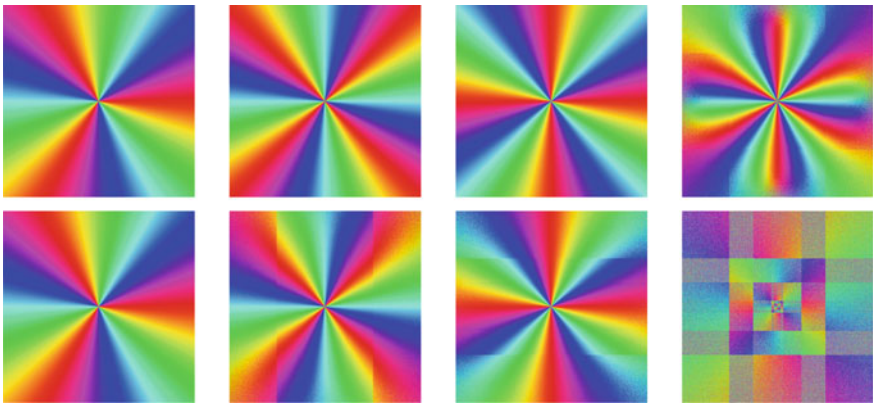

Fig. 19 Error functions for numerical differentiation

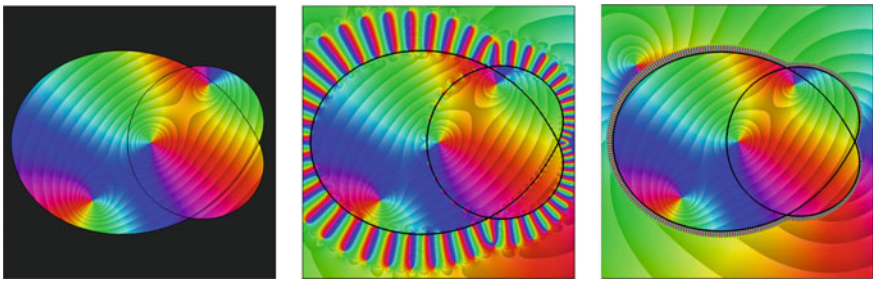

Fig. 20 Evaluation of Cauchy integrals

computer expert the emerging structure may reveal information about the implemented arithmetic).

The most interesting observation is that one can read off the approximation order n directly: applying the method to $f(z) = z^{-1}$, the resulting phase plot shows a pole of order $n + 2$ at the origin. Similar types of experiments can be designed for other approximation methods.

4.6.3 Numerical Integration

Evaluation of integrals is another topic which can nicely be illustrated and studied using phase plots. In Fig. 20, we demonstrate this for a Cauchy integral of an analytic function f. The exact values of the integral are displayed in the figure on the left-hand side. Outside the contour of integration the integral vanishes, at points z surrounded by the contour its values are equal to $k\, f(z)$, where k is the winding number of the contour about z (here k is either 1 or 2).

The other two figures show approximations of the integral, evaluated by the trapezoidal rule with 200 and 1200 nodes, respectively. We see poles, sitting at the contour of integration, induced by the pole of the Cauchy kernel. The gear-like pattern in the exterior domain has almost parallel isochromatic lines, indicating rapid decay of the function (in the direction perpendicular to the contour); it is bounded by a chain of zeros aligned along the contour of integration. This chain may be related to Jentzsch's theorem and its generalizations ([8, 20, 46]).

Austin, Kravanja and Trefethen [1] used phase plots in order to compare different methods (Cauchy integrals, polynomial and rational interpolation) for computing values $f(z)$ and $f^{(m)}(z)$ of analytic and meromorphic functions in a disk from samples at the boundary of that disk.

4.6.4 Padé Approximation

Phase plots of rational functions can "visually approximate" any image, drawn solely with saturated colors from the hsv color wheel (for a precise statement see [50]). Particularly nice images arise from rational functions with zeros and poles forming special patterns, as it happens, for instance, in Padé approximation. In turn, these images may help to understand special aspects of these approximations.

The first row of Fig. 21 shows the function $f(z) = \tan z^4$ to be approximated (left), and two Padé approximants of order [100, 100]. The function depicted in the middle is computed by a standard method, the function on the right is the output of a stabilized ("robust") algorithm developed by Gonnet et al. [17]. Though the pictures can barely be distinguished, the structural differences become obvious in the next two rows, depicting phase plots of the numerator polynomial p (left) and the denominator polynomial q (middle), as well as the error function $f - f_{[100,100]}$ (right). The upper row corresponds to the standard algorithm, while the lower row visualizes the output of the stabilized algorithm. Apparently the first one produces a lot of spurious zeros in both polynomials p and q, which are (almost) canceled in the quotient p/q.

The black line in the error plots on the right-hand side is the unit circle. The almost(!) unstructured part in the middle (the influence of the zero-pole-cancelation is seen here) is due to small fluctuations about zero.

The computations are performed with the Matlab routine `padeapprox` of the Chebfun toolbox (for details see [17]).

4.6.5 Differential Equations

Numerous classes of special functions (Bessel, Airy, hypergeometric, etc.) arise as solutions of second order ordinary differential equations (ODEs). Computing these functions often requires elaborate numerical methods. A particularly hard case is given by the six Painlevé equations, which are prototypes of equations

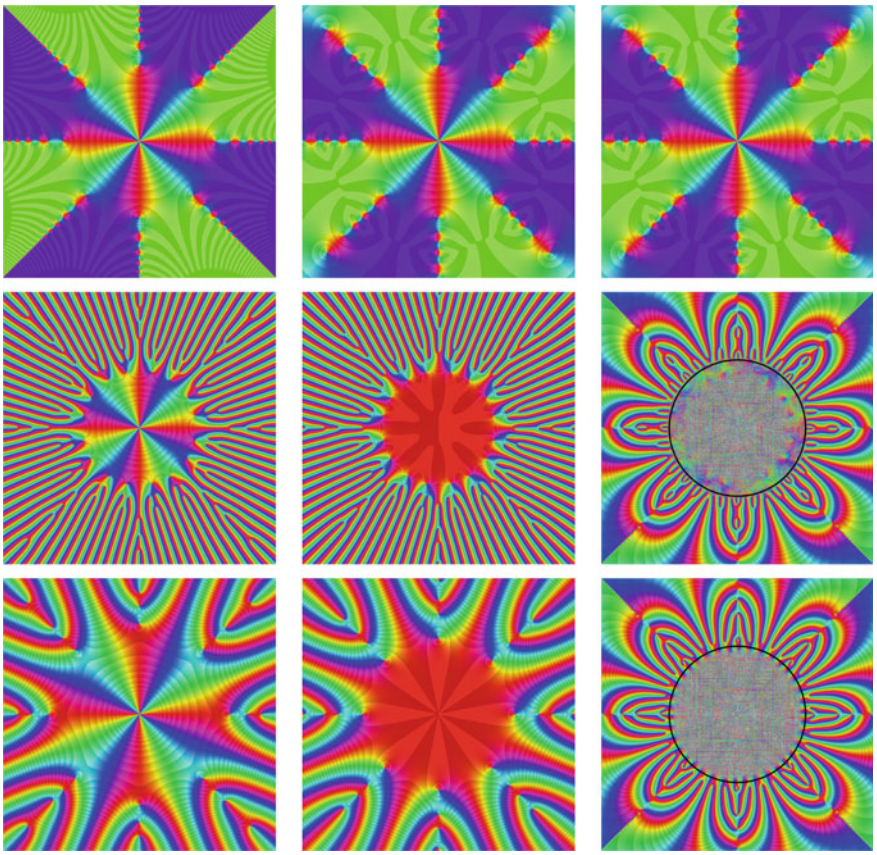

Fig. 21 Padé approximation of $f(z) = \tan z^4$

$$u'' = F\left(z, u, u'\right),$$

where F is a rational function of its arguments, and have single-valued solutions u for all choices of their two initial conditions.

Solutions of Painlevé equations often have widely scattered poles, which were for a long time perceived as "numerical mine fields." Only in 2011, the first effective numerical algorithm for calculating their solutions was described by Bengt Fornberg and Andre Weideman [14].

Figure 22 shows special solutions of the Painlevé I (left) and Painlevé II equation (right), computed by Fornberg and Weideman (I am grateful to the authors for providing the data). The phase plot does not only deliver much more information than the plain zero-pole-pattern usually displayed in texts about Painlevé equations—one does not even need *compute* the zeros and poles, they show up automatically.

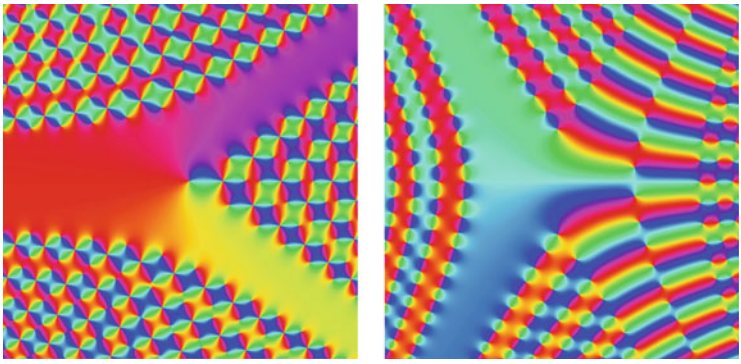

Fig. 22 Solutions of the Painlevé I and II equations

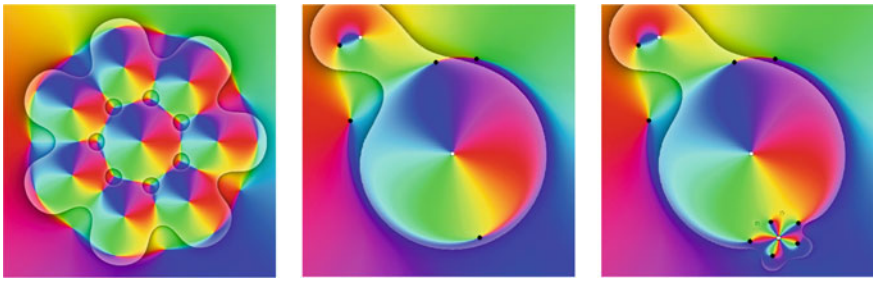

Fig. 23 Rational harmonic functions in gravitational lensing

4.7 Gravitational Lensing

Though phase plots allow one only to reconstruct meromorphic functions (almost) uniquely, they may nevertheless help to explore more general classes of functions. As an example we consider a problem involving *rational harmonic* functions which arises in gravitational lensing.

In 2006, Dmitri Khavinson and Genevra Neumann [22] proved that functions of the form $f(z) = r(z) - \overline{z}$, where r is a rational function of degree $n \geq 2$, can have at most $5n - 5$ zeros. That this bound is sharp follows from an example given by the astrophysicist Sun Hong Rhie in 2003. In the context of her paper [35], the zeros of f represent the images produced from a single light source by a gravitational lens formed by n point masses, located at the n poles of $r(z)$.

The picture on the left of Fig. 23 is a phase plot of Rhie's example for $n = 8$, having 35 zeros. Due to the term $\overline{z}$, the function f is not meromorphic, and hence a pure phase plot does not depict all properties one is interested in. The modified color scheme of the image allows one to read off where the mapping $z \mapsto f(z)$ is orientation preserving (brighter colors) or orientation reserving (darker colors). This is important to distinguish between zeros and poles: in the brighter regions the

orientation of colors near a zero of f is the same as in the color wheel; in the darker regions the orientation is reversed.

Rhie's example was highly symmetric, and it is very unlikely that heavy cosmic objects (galaxies) form such a pattern. So it was greatly appreciated by the community of astrophysicists when Robert Luce, Olivier Sète and Jörg Liesen [37, 38] found a more general recursive construction of maximal gravitational lenses without symmetry. Phase plots played a prominent role in their investigations see [25]. The two images on the right of Fig. 23 (provided by the authors) illustrate how five zeros emerge from introducing an additional pole near a former zero located in the orientation preserving region of f.

4.8 The Riemann Zeta Function

Without doubt the Riemann Zeta function is one of the most fascinating mathematical objects. A reformulation of Bagchi's general universality theorem ([2, 21]) implies that its phase plot in the right half $1/2 < \operatorname{Re} z < 1$ of the critical strip is incredibly colorful (see [53]). Figure 24 displays a collection of phase plots of Zeta in the critical strip. Each rectangle has width 1 and covers about 20 units in the direction of the imaginary axis, with some overlap between neighboring rectangles. Since our visual system is trained in pattern detection, it usually does not take long until one discovers a diagonal structure. This observation inspired Jörn Steuding and me to study mean values of the Zeta function on (vertical) arithmetic progressions. Sampling ζ at points with fixed distance d, we expected that the asymptotic behavior of the mean values should be nontrivial if d is in resonance with the observed stochastic period. This could be confirmed by the following result from our paper [41].

Theorem 4.1 *Fix $s \in \mathbb{C} \setminus \{1\}$ with $0 < \sigma := \operatorname{Re} s \le 1$, $t := \operatorname{Im} s \ge 0$, and let $d = 2\pi/\log m$, where $m \ge 2$ is an integer. Then, for $M \to +\infty$,*

$$\frac{1}{M} \sum_{0 \le k < M} \zeta(s + \mathrm{i}k\,d) = \frac{1}{1 - m^{-s}} + O(M^{-\sigma} \log M).$$

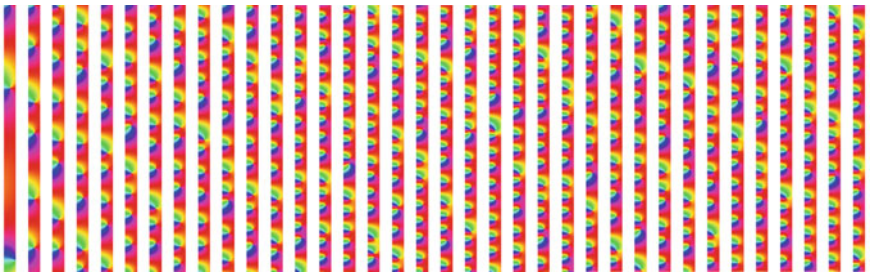

Fig. 24 The Riemann Zeta function in the critical strip

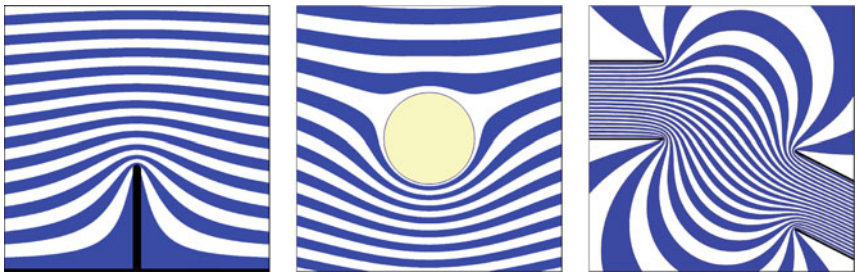

Fig. 25 A color scheme for generating stream lines

We point out that this result does not really explain the observed stripes (which correspond to $d = 2$). To do this, one should consider mean values of the *phase* of Zeta instead of Zeta itself—another challenging problem ….

5 Concluding Remarks

Visualization of complex functions may facilitate new views on known results, raise interesting questions at all levels of difficulty, and, as the last example has shown, may inspire research.

Besides phase plots and standard domain coloring many other color schemes may be useful to illustrate and investigate special features of a function. So the striped patterns in Fig. 25 are convenient to display flow lines, while the chess-board-like structures in Fig. 26 are more appropriate to visualize conformal mappings. In this figure, the domain of the mapping is displayed in the upper row, while the lower row shows the corresponding image domains.

Cristina Ballantine and Dorin Ghisa [3, 4] used very beautiful color schemes to visualize Blaschke products, and Ghisa [16] analyzes several special functions (including the Gamma function and Riemann's Zeta function) using their coloring techniques.

Going a step further, one can put any image in the range plane of a complex function and pull it back to the domain, which may have fascinating and appealing results. For some masterpieces (and the theoretical background) we refer to Frank Farris work [12, 13].

Applications of phase plots in teaching comprise the visualization of converging power series, Weierstrass' disk chain method, Riemann surfaces, and other topics of standard lectures on complex functions. With *dynamic phase plots* one can interactively study the dependence of functions on parameters—such hands-on approaches allow students to become familiar with abstract concepts by doing their own experiments.

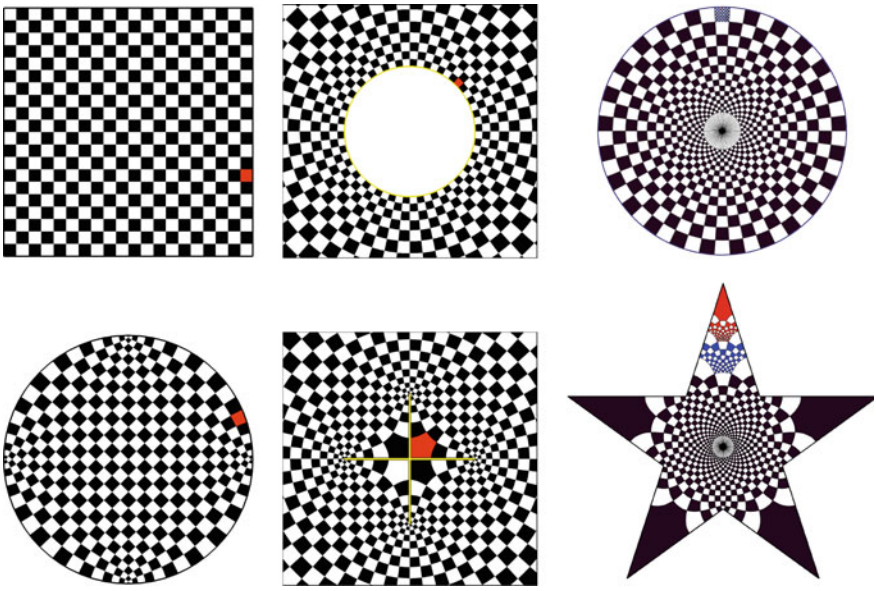

Fig. 26 Color schemes for visualizing conformal mappings

A comprehensive teaching-oriented introduction to complex functions and phase plots is given in the author's textbook [49]. A mathematical calendar featuring this theme can be downloaded at [54].

Matlab software for generating phase plots and colored analytic landscapes on plain domains and the Riemann sphere with various color schemes is available at the Matlab exchange platform [51, 52]. For implementations in Mathematica, we refer to Thaller [42], Trott [44], Sandoval-Romero and Hernández-Garduño [36], and Shaw [39]. Visual Basic code can be downloaded from Larry Crone's website [9]. A stand-alone Java implementation of phase plots of elementary functions is available as part of the Cinderella project by Ulrich Kortenkamp and Jürgen Richter-Gebert [23].

References

1. Austin, A.P., Kravanja, P., Trefethen, L.N.: Numerical Algorithms based on analytic function values at roots of unity. SIAM J. Numer. Anal. **52**, 1795–1821 (2014)
2. Bagchi, B.: A universality theorem for Dirichlet L-functions. Mat. Z. **181**, 319–334 (1982)
3. Ballantine, C., Ghisa, D.: Color visualization of Blaschke self-mappings of the real projective plane. Rev. Roum. Math. Pures Appl. **54**, 375–394 (2009)
4. Ballantine, C., Ghisa, D.: Colour visualization of Blaschke product mappings. Complex Var. Elliptic Equat. **55**, 201–217 (2010)
5. Banchoff, T.: Complex function graphs. http://www.math.brown.edu/~banchoff/gc/script/CFGInd.html

6. Belyi, G.V.: Galois extensions of a maximal cyclotomic field. Izvestiya Akademii Nauk SSSR **14**, 269–276 (1979). (Russian). English translation: Mathematics USSR Izvestija, **14**, 247–256 (1980)
7. Bordignon, A.L., Sa, L., Lopes, H., Pesco, S., de Figueiredo, L.H.: Point-based rendering of implicit surfaces in R4. Comput. Graph. **37**, 873–884 (2013)
8. Blatt, H.P., Blatt, S., Luh, W.: On a generalization of Jentzsch's theorem. J. Approx. Theory **159**, 26–38 (2009)
9. Crone, L.: Color graphs of complex functions. http://www1.math.american.edu/People/lcrone/ComplexPlot.html Accessed 17 Mar 2016
10. Farris, F.A.: Review of Visual Complex Analysis. By Tristan Needham. Am. Math. Monthly **105**, 570–576 (1998)
11. Farris, F.A.: Visualizing complex-valued functions in the plane. http://www.maa.org/visualizing-complex-valued-functions-in-the-plane (2016). Accessed 17 Mar 2016
12. Farris, F.A.: Symmetric yet organic: Fourier series as an artist's tool. J. Math. Arts **7**, 64–82 (2013)
13. Farris, F.A.: Creating Symmetry: The Artful Mathematics of Wallpaper Patterns, 230p. Princeton University Press (2015)
14. Fornberg, B., Weideman, J.A.C.: A Numerical methodology for the Painlevé equations. J. Comput. Phys. **230**, 5957–5973 (2011)
15. Garrido, S., Moreno, L.: PM diagram of the transfer function and its use in the design of controllers. J. Math. Syst. Sci. **5**, 138–149 (2015)
16. Ghisa, D.: Fundamental Domains and the Riemann Hypothesis, 148p. Lap Lambert Academic Publishing (2012)
17. Gonnet, P., Güttel, S., Trefethen, L.N.: Robust Padé approximation via SVD. Siam Rev. **55**, 101–117 (2013)
18. Hernández, M.A.: An acceleration procedure of the Whittaker method by means of convexity. Zb. Rad. Prirod.-Mat. Fak. **20**, 27–38 (1990)
19. Jahnke, E., Emde, F.: Funktionentafeln mit Formeln und Kurven. Teubner (1933)
20. Jentzsch, R.: Untersuchungen zur Theorie der Folgen analytischer Funktionen. Acta. Math. **41**, 219–251 (1918)
21. Karatsuba, A.A., Voronin, S.M.: The Riemann Zeta-Function. Walter de Gruyter (1992)
22. Khavinson, D., Neumann, G.: From the fundamental theorem of algebra to astrophysics: a "harmonious" path. Not. AMS **55**, 666–675 (2008)
23. Kortenkamp, U., Richter-Gebert, J.: Phase Diagrams of Complex Functions. http://science-to-touch.com/CJS/CindyJS/complexFunctions/ (2016). Accessed 17 Mar 2016
24. Kranich, S.: Continuity in dynamic geometry. An algorithmic approach. Ph.D. thesis, TU Munich (2016)
25. Luce, R., Sète, O., Liesen, J.: A note on the maximum number of zeros of $r(z) - \overline{z}$. Comput. Methods Funct. Theory **15**, 439–448 (2015)
26. Lundmark, H.: Visualizing complex analytic functions using domain coloring. http://users.mai.liu.se/hanlu09/complex/domain_coloring.html (2016). Accessed 18 Mar 2016
27. Marshall, D.E.: Conformal welding for finitely connected regions. Comput. Methods Funct. Theory **11**, 655–669 (2011)
28. Marshall, D.E.: Conformal welding and planar graphs. http://www.birs.ca/events/2015/5-day-workshops/15w5052/videos/watch/201501120953-Marshall.html (2016). Accessed 15 Mar 2016
29. Marshall, D.E.: Numerical conformal mapping software: zipper. https://www.math.washington.edu/~marshall/zipper.html (2016). Accessed 15 Mar 2016
30. Marshall, D.E., Rohde, S.: Convergence of a variant of the Zipper algorithm for conformal mapping. SIAM J. Numer. Anal. **45**, 2577–2609 (2007)
31. Maillet, E.: Sur les lignes de décroissance maxima des modules et les équations algébraiques ou transcendantes. J. de l'Éc. Pol. **8**, 75–95 (1903)
32. Nieser, M., Poelke, K., Polthier, K.: Automatic generation of Riemann surface meshes. In: Advances in Geometric Modeling and Processing. Lecture Notes in Computer Science, vol. 6130, pp. 161–178. Springer (2010)

33. Poelke, K., Polthier, K.: Lifted domain coloring. Comput. Graph. Forum **28**, 735–742 (2009)
34. Poelke, K., Polthier, K.: Domain coloring of complex functions: an implementation-oriented introduction. IEEE Comput. Graphics Appl. **32**, 90–97 (2012)
35. Rhie, S.H.: n-point gravitational lenses with 5(n-1) images. ArXiv Astrophysics arXiv:astro-ph/0305166 (2003)
36. Sandoval-Romero, Á., Hernández-Garduño, A.: Domain coloring on the riemann sphere. Math. J. **17** (2015)
37. Sète, O., Luce, R., Liesen, J.: Perturbing rational harmonic functions by poles. Comput. Methods Funct. Theory **15**, 9–35 (2015)
38. Sète, O., Luce, R., Liesen, J.: Creating images by adding masses to gravitational point lenses. Gen. Relativ. Gravit. **47**, 42 (2015)
39. Shaw, W.T.: Complex Analysis with Mathematica. Cambridge University Press (2006)
40. Stefan, M.B.: On doubly periodic phases. Proc. Am. Math. Soc. **142**, 3149–3152 (2011)
41. Steuding, J., Wegert, E.: The Riemann zeta function on arithmetic progressions. Exp. Math. **21**, 235–240 (2012)
42. Thaller, B.: Visualization of complex functions. Math. J. **7**, 163–180 (1999)
43. Trott, M.: Visualization of Riemann surfaces of algebraic functions. Math. Educ. Res. **6**, 15–36 (1997)
44. Trott, M.: Visualization of Riemann surfaces. http://library.wolfram.com/infocenter/Demos/15/ (2016). Accessed 17 Mar 2016
45. Varona, J.L.: Graphic and numerical comparison between iterative methods. Math. Intell. **24**, 37–46 (2002)
46. Walsh, J.L.: The location of critical points of analytic and harmonic functions. American Mathematical Society Colloquium Publications **34**, 386p, New York (1950)
47. Walsh, J.L.: Note on the location of zeros of extremal polynomials in the non-Euclidean plane. Acad. Serbe Sci. Publ. Inst. Math. **4**, 157–160 (1952)
48. Wegert, E.: Phase diagrams of meromorphic functions. Comput. Methods Funct. Theory **10**, 639–661 (2010)
49. Wegert, E.: Visual Complex Functions. An Introduction with Phase Portraits. Springer Basel (2012)
50. Wegert, E.: Complex functions and images. Computational Methods and Function Theory **13**, 3–10 (2013)
51. Wegert, E.: Phase plots of complex functions. http://www.mathworks.com/matlabcentral/fileexchange/44375 (2016). Accessed 15 Mar 2016
52. Wegert, E.: The complex function explorer. http://www.mathworks.com/matlabcentral/fileexchange/45464 (2016). Accessed 15 Mar 2016
53. Wegert, E., Semmler, G.: Phase plots of complex functions: a journey in illustration. Not. AMS **58**, 768–780 (2011)
54. Wegert, E., Semmler, G., Gorkin, P., Daepp, U.: Complex Beauties. Mathematical calendars featuring phase plots. http://www.mathcalendar.net (2016). Accessed 15 Mar 2016
55. Wolfram Research, The Wolfram Functions Site. http://www.functions.wolfram.com (2016). Accessed 15 Mar 2016